Main Manuscript for

Skeletal progenitor LRP1-mediated endocytosis is critical for synovial joint formation and bone growth

Mohammad Alhashmi, Abdulrahman ME Gremida, Noor A Al-Maslamani, Ke Liu, Hazel Sutherland, Peter Wilson, Peter Clegg, Robert J van 't Hof, George Bou-Gharios and Kazuhiro Yamamoto*.

Institute of Life Course and Medical Sciences, University of Liverpool.

Corresponding author: Kazuhiro Yamamoto
William Henry Duncan Building,
University of Liverpool, 6 West Derby Street,
Liverpool, L7 8TX, UK.
kazuhiro.yamamoto@liverpool.ac.uk

Keywords: Skeletal development/ endocytosis/ perichondrium/ morphogen gradient/ extracellular matrix.

This PDF file includes:

Main Text
Figures 1 to 7

Abstract

The layer of stem cells surrounding developing limbs is essential for bone formation and regeneration. Our work addresses the critical question of how these stem cells and bone template communicate to ensure that limbs form correctly. Low-density lipoprotein receptor-related protein 1 (LRP1) is a multifunctional endocytic receptor whose mutations are linked to bone and joint pathologies. Here, we show the abundant expression of LRP1 in skeletal progenitor cells, especially in the perichondrium – the dense layer of fibrous connective tissue enveloping the cartilage of the developing limb bud. Our mouse models reveal that LRP1 deficiency in these stem cells ($Lrp1^{flox/flox}/Prrx1^{Cre}$) but not in chondrocytes ($Lrp1^{flox/flox}/Acan^{CreERT2}$) causes disrupted articulation and cavitation starting at as early as embryonic stage 16.5. LRP1 deficiency is also associated with aberrant accumulation of LRP1 ligands including tissue-inhibitor of metalloproteinase 3 and CCN2. These early abnormalities result in severe defects in multiple joints, plus markedly deformed and low-density long bones leading to dwarfism and impaired mobility. Our *in vitro* exploration shows unique regulation of non-canonical WNT components by LRP1 that may explain the malformation of long bones. Mechanistically, we found that LRP1 facilitates cell-association, endocytic recycling but not degradation, and graded distribution of Wnt5a in the developing limbs. We propose that LRP1-mediated endocytic regulation of availability and distribution of extracellular signalling molecules play a critical role in limb development. This provides a novel mechanism for crosstalk among skeletal elements.

Main Text

Introduction

Studies on vertebrate limb development have illuminated many common principles that orchestrate organogenesis. The perichondrium is a dense layer of fibrous connective tissue that covers cartilage in endochondral ossification. Compared to chondrocyte growth plates and those of the articular cartilage lining joints, little is known about the perichondrium albeit it appears to have two broad functions. First, perichondrial cells signal to underlying chondrocytes and receive signals from these cells in turn. Second, they provide cells that become osteoblasts and chondrocytes in a carefully orchestrated fashion. However, questions remain regarding molecular mechanisms underpinning cellular communication between the perichondrial cells and bone template.

Low-density lipoprotein (LDL) receptor-related protein 1 (LRP1) is a ubiquitously expressed type 1 transmembrane protein that mediates clathrin-dependent endocytosis of structurally and functionally diverse molecules (Bres and Faissner, 2019; Strickland et al., 2002). LRP1 is also involved in modulation of cellular signalling pathways by binding to extracellular ligands and subsequent intracellular interaction with scaffolding and adaptor proteins. Global deletion of the *Lrp1* gene in mice results in early embryonic lethality at E13.5 (Herz et al., 1992; Nakajima et al., 2014). The homozygous and even heterozygous *Lrp1* null$^{tm1.1(KOMP)Wtsi}$ mice exhibit multiple phenotypes, as described in the Mouse Genome Informatics database (MGI: 5495233). These studies indicate a critical, but as yet unknown role of LRP1 in development. In adult mice, tissue specific *Lrp1* deletion has revealed various biological roles of LRP1 including lipoprotein metabolism (Ding et al., 2016; Hamlin et al., 2016), insulin signalling (Hofmann et al., 2007), vascular wall integrity (Boucher et al., 2003; Mao et al., 2016; Muratoglu et al., 2013), inflammation (Hu et al., 2006; Overton et al., 2007) and bone remodelling (Bartelt et al., 2018; Lu et al., 2018; Vi et al., 2018).

We have previously shown that LRP1 plays a key role in maintaining the extracellular matrix (ECM) turnover in healthy adult cartilage (Carreca et al., 2020; Scilabra et al., 2013b; Scilabra et al., 2017; Troeberg et al., 2008; Yamamoto et al., 2016; Yamamoto et al., 2014; Yamamoto et al., 2013). This endocytic process is impaired in cartilage under inflammatory conditions or in osteoarthritis (OA), the most prevalent age-related degenerative joint disease (Yamamoto et al., 2017). Realising the importance of LRP1 in cartilage biology, we have recently identified chondrocyte-specific LRP1 ligands including growth factors, morphogens, inflammatory mediators, hyaluronan-binding proteins, matricellular proteins, ECM proteins, proteinases and proteinase

inhibitors (Yamamoto et al., 2022), highlighting the extent and tissue/cell-dependent function of LRP1.

LRP1 single nucleotide polymorphisms have been associated with a decreases in bone mineral density and content (Sims et al., 2008). A recent study by Yan *et al* (Yan et al., 2022) identified mutations in *LRP1* in developmental hip dysplasia (DHD) patients. Their mouse equivalent model showed delayed Y-shaped triradiate cartilage development and smaller acetabulum sockets in 16-weeks old mice compared to control mice. Heterozygous global *Lrp1* knockout (KO) mice also developed a hip dysplasia phenotype, whilst homozygous *Lrp1* KO mice (*Lrp1*$^{flox/flox}$*/Col2a1*^{Cre}) showed shortened bones and cartilage growth plate (Mark et al., 2022). However, when and where LRP1 is expressed and how LRP1 deletion leads to these pathologies during skeletal development are not fully understood.

In this study, we showed that LRP1 is abundantly expressed in early skeletal progenitor cells, in particular in the perichondrium. To investigate the role of perichondrial LRP1, we generated a conditional KO of *Lrp1* using paired-related homebox gene-1 (*Prrx1*), which is expressed in the early limb bud skeletal mesenchyme and a subset of craniofacial mesenchyme (Cserjesi et al., 1992; Martin and Olson, 2000). We also explored molecular mechanisms underpinning the multiple severe skeletal defects observed in *Lrp1*$^{flox/flox}$*/Prrx1*^{Cre} mice. Our data show that perichondrial LRP1 is critical for endochondral ossification and that it uniquely regulates Wnt morphogens. This suggests that LRP1 plays a critical role in communication between the perichondrium and limb template.

Results

LRP1 is abundantly expressed in periosteal and perichondrial stem cells.

Histological investigation of LRP1 protein in adult knee joint tissue revealed that LRP1 was abundantly expressed in articular chondrocytes, cells in ligaments, medial meniscus, synovial membranes, trabecular bones and skeletal muscles (**Fig 1A**). A particularly strong LRP1 immunosignal was detected in the layers of cells surrounding femur and tibia, namely the periosteum. These immunosignals were markedly diminished in the inducible pan-tissue *Lrp1* KO mice (*Lrp1*$^{flox/flox}$*/ROSA26*$^{Cre/ERT2}$), confirming specificity of the LRP1 immunostaining. Histological analysis of 14-week-old femoral head confirmed abundant expression of LRP1 in the periosteum as well as articular chondrocytes in superficial zone (**Fig 1B**). The perichondrium in the developing cartilage and bone transforms into periosteum (Ono et al., 2019). We therefore tested LRP1

expression across embryonic stages. Notably, LRP1 is abundantly expressed in E13.5- to newborn (P0) elbow joints, with the strongest immunosignals of LRP1 detected in the perichondrium layers (**Fig 1C**). This suggests a possible role of LRP1 in crosstalk between the limb template and the perichondrium.

Conditional deletion of *Lrp1* in skeletal progenitors but not in chondrocytes impairs early bone and joint formation.

To investigate the role of perichondrial LRP1 in skeletal development *in vivo*, we have established a double transgenic mouse line *Lrp1*$^{flox/flox}$*/Prrx1*^{Cre} (**Fig 2A**). In this strain, a 2.4 kb *Prrx1* enhancer directs the transgene expression in undifferentiated mesenchyme in the developing limb buds around embryonic day 9.5 (E9.5) (Cserjesi et al., 1992; Kawanami et al., 2009; Logan et al., 2002; Martin and Olson, 2000). Transgene expression is extinguished in the condensing mesenchyme and chondrocytes, and the expression is confined to the perichondrium/periosteum of the limbs at E15.5. Immunohistochemistry of LRP1 confirmed that LRP1 immunosignals were specifically diminished in *Prrx1* expressing cells in the E16.5 knee but not in their ribs (**Fig 2B**). Western blot analysis of cells isolated from 5-week-old wild-type (WT) and *Lrp1*$^{flox/flox}$*/Prrx1*^{Cre} long bones further confirmed an efficient deletion of LRP1 protein in *Lrp1*$^{flox/flox}$*/Prrx1*^{Cre} mice (**Fig 2C**).

Haematoxylin and eosin (H&E) staining of limbs at different embryonic stages showed that articulation defects were clearly observed in shoulder, elbow and knee joints at E16.5 homozygote mice (**Fig 2D-F**) and the defects become more severe in E18.5 and P0 mice (**Fig 2EF**). Striking articulation defects were observed in P0 *Lrp1*$^{flox/flox}$*/Prrx1*^{Cre} hip joints (**Fig 2G**). These defects were not observed in heterozygote (*Lrp1*$^{flox/wt}$*/Prrx1*^{Cre}) littermates. Histological investigation of LRP1 ligands including tissue inhibitor of matrix metalloproteinase 3 (TIMP3) and CCN2 revealed their aberrant accumulation in P0 *Lrp1*$^{flox/flox}$/*Prrx1*^{Cre} compared to WT limbs (**Fig 2HI**). High resolution µCT scanning further showed that femur and humerus length were shorter in P0 *Lrp1*$^{flox/flox}$*/Prrx1*^{Cre} compared to WT mice, whereas no significant difference was observed in E18.5 mice (**Fig 2J**). No significant differences in body and skull length were observed in P0 mice (**Fig 2K**).

To investigate whether chondrocyte LRP1 is responsible for the cKO skeletal phenotype, we generated double transgenic mice line *Lrp1*$^{flox/flox}$*/Acan*^{CreERT2} (Henry et al., 2009). In contrast to *Prrx1* expression (Logan et al., 2002; Martin and Olson, 2000), *Aggrecan* expression was detected in the E13.0 forelimb and in all developing cartilage by E15.5 (Henry et al., 2009). *Lrp1* was deleted at the different embryonic stages and E19.5 embryos were examined (**Fig S1**). *Lrp1* gene excision was confirmed by *Lrp1 exon 2* PCR (**Fig S1B**) but histological analysis and bone length measurement

confirmed normality of skeletal development in E19.5 *Lrp1*$^{flox/flox}$/*Acan*^{CreERT2} mice (**Fig S1C-F**). These results suggest that LRP1 in skeletal precursors but not in chondrocytes plays a pivotal role in early skeletogenesis.

LRP1 deficiency in skeletal progenitors results in dwarfism, impaired mobility and multiple severe skeletal defects.

We next investigated the impact of early skeletal developmental defects in postnatal *Lrp1*$^{flox/flox}$/*Prrx1*^{Cre} mice. The mice survived into adulthood, but the weight of the homozygote mice was consistently lower than their WT and heterozygote littermates starting 3 weeks up to 14 weeks after birth (**Fig 3A**). Strikingly, *Lrp1*$^{flox/flox}$/*Prrx1*^{Cre} mice consistently showed altered posture and impaired mobility at birth which was persistent up until 14 weeks of age (**Movies S1 and S2**). A continuous automated home-cage monitoring system for a 4-week period from week 6 showed significantly reduced locomotor activity of *Lrp1*$^{flox/flox}$/*Prrx1*^{Cre} mice compared with WT littermates (**Figure 3B**). Whole-mount skeletal staining of 14-week-old postnatal adult mice with Alcian blue and Alizarin red showed that *Lrp1*$^{flox/flox}$/*Prrx1*^{Cre} mice had shorter limbs and smaller stature than their WT littermates (**Fig 3C**).

In vivo µCT scanning of 2-week-old *Lrp1*$^{flox/flox}$/*Prrx1*^{Cre} mice revealed that long bones were not only shorter but markedly thicker and twisted, with much delayed emergence of secondary ossification centres (**Fig 3D**). The upper limbs were abnormally twisted and the scapular were poorly defined compared to WT. The absence of crescent acetabulum sockets, rounded femoral heads and patella bone in *Lrp1*$^{flox/flox}$/*Prrx1*^{Cre} mice suggests a mechanism for the impaired mobility. These bone deformities could still be observed in 14-week-old mice (**Fig 3E**). The observed difference in the length and width of femur and humerus bones between 6-week-old WT and *Lrp1*$^{flox/flox}$/*Prrx1*^{Cre} mice persisted in 14-week-old mice (**Fig 3F** and **S2**). We also found a substantial reduction in trabecular bone density in 14-week-old *Lrp1*$^{flox/flox}$/*Prrx1*^{Cre} tibia with virtual absence of primary spongiosa compared to the WT tibia (**Fig 3G**). None of these phenotypes were observed in the heterozygote mice, further supporting the notion that both haplotypes were needed for this phenotype.

LRP1 deficiency in skeletal progenitors disrupts growth plate and columnar chondrocyte organisation, impairs articulation and cavitation, and dysregulates proteoglycan turnover.

To explore the mechanisms behind the multiple and severe skeletal defects in *Lrp1*$^{flox/flox}$/*Prrx1*^{Cre} mice, we further histologically examined the bone and joint sections. Dynamic histomorphometry of

bone formation using calcein-double labelling in 14-week-old mice showed a comparable bone formation rate between WT and *Lrp1*$^{flox/flox}$/*Prrx1*^{Cre} mice (**Fig 4A** and **S3A-C**). Tartrate-resistant acid phosphatase (TRAP) staining for osteoclasts revealed approximately 1.9-fold increased osteoclast activity in 14-week-old *Lrp1*$^{flox/flox}$/*Prrx1*^{Cre} mice compared to WT littermates (**Fig 4BC** and **S3DE**). These results are consistent with *Lrp1* deficiency in osteoblasts (Bartelt et al., 2018) or osteoclasts (Lu et al., 2018) resulting in low bone-mass phenotype due to increased osteoclastogenesis.

H&E staining of 2- and/or 14-week-old *Lrp1*$^{flox/flox}$/*Prrx1*^{Cre} shoulder, elbow and knee revealed striking defects (**Fig 4D-F**). These included a deformed and disrupted growth plate with poorly stacked columnar chondrocytes, markedly delayed secondary ossification, impaired articulation and fused articular cartilage without sphere-shape or smoothness. Safranin-O/fast green staining further revealed proteoglycan depletion in articular cartilage and the growth plate in 14-week-old mice but not 2-week-old mice (**Fig 4D-F**). Similar results were also obtained by Toluidine blue staining. Notably, femoral heads were substantially deformed with an extra groove juxtaposed to a poorly developed acetabulum socket (**Fig 4G**). Immunohistochemical staining of Sox9, a pivotal transcription factor expressed in developing and adult cartilage (Akiyama et al., 2002; Bi et al., 1999; Haseeb et al., 2021), was absent in the articular cartilage and growth plate of 14-week-old *Lrp1*$^{flox/flox}$/*Prrx1*^{Cre} mice (**Fig 4H**), emphasising defects in cartilage development.

LRP1 directly binds to Wnt5a and Wnt11, key non-canonical WNT pathway components, and mediates endocytosis of Wnt5a.

The observed skeletal defects could potentially arise from a range of mechanisms. Markedly thicker and shorter long bones (**Fig 3**), and disrupted growth plate with disorganised columnar chondrocytes (**Fig 4**) closely resemble phenotypes associated with defects in the non-conical WNT/planar cell polarity (PCP) pathway (**Fig 5A**)(Galea et al., 2021). For example, deletion of core components of WNT/PCP including *Ror2* (Green et al., 2008), *Vangl2* (Gao et al., 2011), the receptor-like tyrosine kinase (Andre et al., 2012) and Wnt5a (Yamaguchi et al., 1999) as well as inducible Wnt5a overexpression (van Amerongen et al., 2012) all result in shorter and thicker long bones. The chondrocyte-specific LRP1 ligand profile shows >50 novel candidate binding partners, including Wnt5a and Wnt11 (Yamamoto et al., 2022). We therefore investigated the potential for direct interaction of Wnt5a and Wnt11 with LRP1 using a solid-phase binding assay. The assay employed purified Wnts and full-length LRP1(Mogensen et al., 2022). We found that Wnt5a and Wnt11 directly bind to immobilised LRP1 with high affinity (apparent binding constant ($K_{D,app}$) of 31

nM and 42 nM, respectively (**Fig 5BC**). In contrast, binding of Wnt3a, a key canonical WNT component, to LRP1 was negligible with $K_{D,app}$ of >200 nM (**Fig 5D**).

Since Wnt5a dysregulation may explain the malformation of long bones, LRP1-mediated endocytosis of Wnt5a was examined in WT and LRP1 KO mouse embryonic fibroblasts (MEFs) (Willnow and Herz, 1994). Immunofluorescent confocal microscopy analysis revealed the co-localisation of Wnt5a and LRP1 inside WT MEFs (**Fig 5E**). The fluorescent signal of Wnt5a was markedly reduced in the LRP1 KO MEFs, indicating that LRP1 mediates internalisation of Wnt5a. The intracellular colocalisation of exogenously added Wnt5a and LRP1 was also observed in human primary chondrocytes (**Fig 5F**). This was markedly reduced in the presence of receptor-associated protein (RAP), which antagonises ligand binding by competitively occupying the ligand binding region of LRP1. Three-dimensional reconstruction of the confocal microscopy images using IMARIS (v8.1) further confirmed that the majority of internalised Wnt5a was associated with LRP1 (**Fig 5H**).

LRP1 facilitates cell-association, endocytic recycling and graded distribution of Wnt5a in the developing limbs.

Several secreted LRP1 ligands are degraded intracellularly following internalisation (Scilabra et al., 2013a; Yamamoto et al., 2016; Yamamoto et al., 2014; Yamamoto et al., 2022; Yamamoto et al., 2013). Some ligands, however, are recycled back to the extracellular milieu, facilitating their distribution and availability (Kawata et al., 2012; Laatsch et al., 2012). We thus monitored the level of exogenously added Wnt5a in the medium and in the cell lysate of WT and LRP1 KO MEFs by Western blot analysis. After 3-24 h incubation, exogenously added Wnt5a was detected in both the conditioned medium and cell lysate (**Fig 5AB**). Notably, no significant difference in Wnt5a levels were observed in LRP1 KO compared to WT MEFs and relatively large amounts of Wnt5a still remained even after 24-h incubation with the cells. We also did not observe rapid endocytic clearance of Wnt5 was also observed in human chondrocytes (**Fig 5C**). To test whether LRP1 facilitates cell-association of Wnt5a through direct capture of Wnt5a, exogenously added Wnt5a was monitored in the cell-lysate for incubation periods ranging between 0-60 min. The levels of cell-bound Wnt5a in WT MEFs after incubation for 5, 15 and 30 min were 1.6, 1.5 and 1.4-fold higher than these in LRP1 KO cells, respectively (**Fig 5DE**). These results suggest that LRP1 facilitates cell-association but not degradation of Wnt5a.

It has been reported that Wnt5a mRNA is expressed in the perichondrium in developing chicken limbs (Church et al., 2002; Hartmann and Tabin, 2000) but Wnt5a protein distribution in the

developing limbs remains incompletely understood. Our histological investigation of Wnt5a protein in E16.5 elbow revealed a Wnt5a distribution pattern similar to that seen for LRP1: abundant expression of Wnt5a in perichondrium and proliferative flattened chondrocytes but very weak expression in hypertrophic chondrocytes (**Fig 5F**). A much less well-defined gradient of Wnt5a in perichondrium and cartilage and bone template was observed in *Lrp1*$^{flox/flox}$/*Prrx1*^{Cre} compared with WT tissue.

Discussion

Two-way signalling between cells in the perichondrium and the underlying cartilage are essential for endochondral bone formation. Our present study revealed an abundant expression of LRP1 in the perichondrium, strongly suggesting a role for LRP1 in the signaling pathways underpinning bond formation. This was confirmed in our conditional *Lrp1* KO models. The severe bone and joint phenotype observed in mice lacking *Lrp1* in skeletal progenitor cells persisted into skeletally mature 14-week-old mice, indicating a critical and non-redundant function of perichondrial LRP1 in skeletal development and maturity. We further demonstrated a regulatory function of LRP1, controlling Wnt5a availability and distribution. This work provides critical insights into how the same morphogen can elicit specific and distinct cellular responses.

Skeletal progenitor LRP1 has at least two different functions: to remove molecules from extracellular milieu and target them for intracellular degradation, and to capture, recycle and distribute molecules (**Fig 7**). Both TIMP3 and CCN2, tightly regulated LRP1 ligands (Scilabra et al., 2013a; Yamamoto et al., 2022), accumulated throughout the ECM in P0 *Lrp1*$^{flox/flox}$/*Prrx1*^{Cre} elbow. This indicated the importance of LRP1 in regulating extracellular concentrations of biologically active LRP1 ligands in the developing limbs. It has been reported that Wnt5a is internalised by cells *via* a clathrin-dependent pathway (Ohkawara et al., 2011; Sato et al., 2010) – raising the possibility of a role for LRP1 in Wnt5a distribution. Our present study identified LRP1, which mediates clathrin-dependent endocytosis, as a major receptor for Wnt5a. Unlike other LRP1 ligands such as TIMP3 (Scilabra et al., 2013a; Troeberg et al., 2008), MMP13 (Yamamoto et al., 2016) and ADAMTS5 (Yamamoto et al., 2013), internalised Wnt5a is not degraded intracellularly, and is most likely recycled. Higher levels of cell-associated Wnt5a were detected in WT compared to LRP1 KO cells, showing that LRP1 effectively captures Wnt5a from the cellular microenvironment. We are currently exploring the possibility that LRP1 facilitates Wnt5a binding to its cell-surface receptor complexes consisting of Ror1/2 and the frizzled receptors (Church and Francis-West, 2002; Hartmann, 2006; Wang et al., 2016). Notably, we found a similar distribution of LRP1 and Wnt5a in the developing

limbs. Their colocalisation in the perichondrium raises the possibility that their interaction controls the recruitment of chondroprogenitor cells from the perichondrium which results in skeletal element widening.

The use of the conditional KO system allowed us to identify at which stage of development we observe changes in the cartilage formation. The abundant expression of LRP1 in skeletal progenitor cells in WT mice, especially in the perichondrium, prompted us to use *Prrx1*^{Cre} to delete *Lrp1* in early skeletal mesenchyme. The histology of homozygous *Lrp1*$^{flox/flox}$/*Prrx1*^{Cre} embryos showed that defects in cartilage articulation and cavitation in shoulder, elbow, hip and knees appear at pre-natal stages, which was not evident in *Lrp1*$^{flox/flox}$/*Acan*^{CreERT2} mice. We concluded that since *Lrp1* deficiency in chondrocytes results in normal joint formation, LRP1 in early skeletal progenitor cells is more intrinsically involved in guiding proper formation of multiple cartilage and bone elements.

Recent evidence for association of LRP1 loss with impaired bone formation was documented in work where homozygous cartilage-selective *Lrp1* KO mice (*Lrp1*$^{flox/flox}$*Col2a1*^{Cre}) and heterozygous global *Lrp1* KO mice developed shortened bones (Mark et al., 2022) and a DHD phenotype (Yan et al., 2022), respectively. In humans, Yan *et al* (Yan et al., 2022) found an association between *LRP1* mutations including R1783W with DHD. In mice, mutant *Lrp1*^{R1783W} homozygote and heterozygote mice exhibited delayed Y-shaped triradiate cartilage and smaller acetabulum in 8-week and 16-week-old mice, respectively (Yan et al., 2022). Our homozygous *Lrp1*$^{flox/flox}$/*Prrx1*^{Cre} mice go beyond the mismatch of the femoral head and acetabulum, and also exhibit lack of proper cavitation in multiple joints including hip, shoulder, elbow and knee, which requires further investigations. In contrast, our heterozygous *Lrp1*$^{wt/flox}$/*Prrx1*^{Cre} mice did not show observable skeletal abnormalities, suggesting that mutations in *LRP1* can be more damaging than deletion especially in cartilage. This is consistent with other findings. For example, mutations in cartilage oligomeric matrix protein (COMP) gene are known to cause pseudo achondroplasia and some types of multiple epiphyseal dysplasia in humans (Briggs et al., 1995; Hecht et al., 1995) but COMP-null mice showed no skeletal phenotype (Svensson et al., 2002). Another illustration of the LRP1 genotype-phenotype variation is tyrosine phosphorylation of the cytoplasmic NPxY motifs within the LRP1 intracellular domain. These motifs provide binding sites for a set of signalling proteins (Barnes et al., 2001; Boucher et al., 2002; Loukinova et al., 2002). Knock-in mouse models of mutation of the proximal, and separately, distal NPxY motif to disable phosphorylation exhibited normal skeletal development (Roebroek et al., 2006), indicating that LRP1 phosphorylation is dispensable for its function in skeletal development.

Since the 2.4 kb *Prrx1* enhancer is reported to be expressed in skeletal muscle at as early as E16.5 (Logan et al., 2002), we cannot exclude the possibility that skeletal muscle LRP1 plays a role in developing the observed phenotype. In particular twisted long bones, can be explained by altered mechanical adaptation due to abnormal skeletal muscle-bone interaction. The cKO mice exhibited significant differences in limb length and femur thickness as early as at P0. One possibility to rationalise drastic skeletal changes at this stage is the mechanical stimuli generated by the embryo's active movements. Embryos with restricted movements in utero showed a skeletal phenotype of reduced ossification, especially in forelimbs (Shea et al., 2015).

The data presented here differ significantly from other LRP family members associated with skeletal formation, such as LRP5 and LRP6, which function as WNT coreceptors with the frizzled receptor and regulate WNT/β-catenin signalling (Pinson et al., 2000; Tamai et al., 2000). LRP5/6 interact with many Wnts (Wnt1/2/3/3a/2b/6/8a/9a/9b/10b) but not Wnt5a or Wnt11 (Ren et al., 2021). *Lrp6* KO mice die at birth and exhibit a variety of severe developmental abnormalities resembling those caused by mutations in Wnt1, Wnt3a and Wnt7a (Pinson et al., 2000). *Lrp6* KO limbs showed a consistent loss of the most posterior digit but did not exhibit the limb outgrowth defects observed in *Wnt5a* KO mice (Yamaguchi et al., 1999). Some *Lrp6* KO mice exhibited deletion of additional digits and the radius, as well as malformation of the ulna. Therefore, the *Lrp1* cKO and *Lrp6* KO phenotypes are distinct.

In conclusion, we showed that LRP1 in early skeletal precursor cells is a critical for synovial joint formation and accurate bone growth, provided a time frame for these events and suggested the mechanisms underpinning the shaping of long bones. We propose that LRP1-mediated endocytosis is a novel mechanism for regulating the distribution of extracellular signalling molecules in cellular communication during skeletal formation. Further investigations into the mechanisms underpinning formation of severe defects in multiple skeletal elements caused by LRP1 loss is a promising approach for understanding the fundamental processes of morphogenesis, as well as the emergence of skeletal pathologies including DHD, osteoporosis and OA.

Materials and Methods

Mice

The *Lrp1*$^{flox/flox}$*/ROSA26*$^{Cre/ERT2}$ strain was established and genotyped as reported previously (Yamamoto et al., 2022). A total 6 homozygotes and 5 WT littermates were examined for this study. For tamoxifen administration, 50 mg tamoxifen free base (SIGMA) was suspended in 500 µl of

100% ethanol, diluted and fully dissolved in 4,500 µl of corn oil (SIGMA) by sonication (final 10 mg/ml). 5 months-old WT and *Lrp1*$^{flox/flox}$/*ROSA26*$^{Cre/ERT2}$ mice were administrated 40 mg tamoxifen/Kg body weight by intraperitoneal injections for three times over a week with 2- and 4-days interval. The mice were culled 3 days after the final dose of tamoxifen. The *Lrp1*$^{flox/flox}$/*Prrx1*^{Cre} mice were generated by crossing the *Lrp1*$^{flox/flox}$ (Strain 012604, the Jackson lab) and *Prrx1*^{Cre} (Strain 005584, the Jackson lab) mice. For post-natal analysis, 22 homozygotes, 14 heterozygotes and 21 wild-type littermates were examined for this study. For embryos, we examined 26 homozygotes, 12 heterozygotes and 24 wild-type littermates were examined for this study.

Mouse genotyping

For genotyping, mice DNA was extracted from ear notches or tails using the RED ExtractN-Amp Tissue PCR Kit (SIGMA). For *Lrp1*^{flox}, following primers were used; forward 5'-CATACCCTCTTCAAACCCCTTCCTG - 3', reverse 5'-GCAAGCTCTCCTGCTCAGACCTGGA - 3' with the following PCR conditions: 1 cycle of 94°C for 3 min, 35 cycles of 94°C for 30 s; 65°C for 30 s; 72°C for 30 s, ended with a final cycle of 72°C for 2 mins. For *Prrx1*^{Cre}, following primers were used, forward 5'- GCTGCCACGACCAAGTGACAGCAA - 3', reverse 5'-CAGTAGCCTCATCATCACTAGATG - 3' with the following PCR conditions: 1 cycle of 94°C for 1 min, 40 cycles of 94°C for 30 s; 60°C for 30 s; 72°C for 1:30 mins; followed by a final cycle of 72°C for 5 mins.

Immunohistochemistry

Slide sections were dewaxed and rehydrated by xylene and decreasing ethanol concentrations. Epitope unmasking was performed using a basic antigen retrieval reagent (R&D systems). The slides were immersed in the basic reagents and kept in a water bath for 10 minutes at 95°C. To block the endogenous peroxidase activity, 0.3% hydrogen peroxide was added to the slides and the slides were kept at 37°C for 15 minutes. Avidin/Biotin blocking kit (Vector Lab) was used to block endogenous biotin, biotin receptors and avidin. To block unspecific antibody binding, 10% goat serum was added to the slides for 3 hours at room temperature (RT). The primary antibody was then added to the slides and kept at 4°C overnight. The impress HRP Goat anti-Rabbit IgG polymer Detection Kit (Vector Lab) was used as a secondary antibody. One drop was used for each section, and the slides were kept at RT for 30 minutes. For signal enhancement, the VECTASTAIN ABC-HRP Kit (Vector Lab) was added to the slides and kept in the dark for 30 minutes. For signal visualisation, the DAB substrate kit (Vector Lab) was used to develop the brown signal. Fast green

was used for counterstaining. Slides were dehydrated, cleared and mounted using increasing concentrations of ethanol, xylene and DPX (SIGMA), respectively. The primary antibodies used were as follows; rabbit monoclonal anti-LRP1 (1:200)(ab92544, Abcam), rabbit polyclonal anti-Sox9 (1:500)(AB5535, SIGMA), rabbit polyclonal anti-Wnt5a (1:200)(bs1948R, Bioss). The Rabbit IgG control antibody (I1000, Vector Lab) was used as isotype control.

Microscopic Examination

For microscopic examination and imaging, the Nikon Eclipse Ci microscope with the DS-Fi2 high-definition colour camera head was used. All images were visualised using NIS-Elements imaging. The Zeiss Axio Scan.Z1 slide scanner system was used for the automated imaging. The resulting images were inspected using ZEN 3.0 (Blue edition), in which the image scale bar was added.

Histology and staining

All samples were fixed with neutral buffered formalin overnight, then kept in 70% ethanol until processing. EDTA was used for bone decalcification with different incubation times based on the samples age. Sample processing was automated using the Leica ASP300 tissue processor (Leica Microsystems, UK). The Leica EG1150 H embedding station was used for sample embedding. Sample sectioning at 5 µm thickness was performed using the Leica RM2245 microtome. For H&E staining, slides were deparaffinised in xylene and rehydrated was performed using decreasing ethanol concentrations. For nucleus staining and counterstaining, slides were stained with haematoxylin and eosin, respectively, for 5 minutes. The slides were then dehydrated in increasing ethanol concentrations before clearing them in xylene followed by mounting. For Safranin O staining, sections were deparaffinised, rehydrated and stained with haematoxylin for 30 seconds followed by counterstaining with 2% fast green for 2 minutes. The sections were then dipped in acetic acid for 20 seconds before staining with safranin O for 8 minutes.

Osteoblast isolation

Upper and lower limb bones from each mouse were chopped into small pieces, followed by collagenase digestion in a shaking water bath for 90 minutes at 37°C. After washing, the crushed bones were resuspended in 2ml of DMEM/F12 media with 10 % Fetal bovine serum (gibco, A384400-01) and then transferred to a T-25 culture flask. Clavaria osteoblasts were harvested the same way, but with collagenase digestion for 180 minutes. Osteoblasts were cultured and then subjected to SDS-PAGE followed by Western blot analysis.

Micro-computed tomography (μCT)

For ex vivo high-resolution μCT imaging, all samples were fixed in buffered formalin and then kept in 70% ethanol until processing. μCT scanning was performed using the Skyscan 1272 (SKYSCAN, Belgium) for all developmental stages. Based on the sample type and age, different imaging parameters were applied. For embryos, the parameters were as follows: 0.5 rotation step, 9μm isotropic resolution, 0.25 aluminium filter, 30 random movements and 4 average frames. For postnatal samples, the scanning parameters were as follows: 0.3 rotation step, 4.5μm isotropic resolution, 0.5 aluminium filter, 30 random movements and 2 average frames. The parameters for skull imaging were as follows: 0.5 rotation step, 9μm isotropic resolution, 0.5mm aluminium filter, 30 random movements and 2 average frames. Skyscan NRecon software was used to reconstruct the obtained images. Skyscan Data Viewer software was used to measure bone length and width. For trabecular bone, the Skyscan CT-analyser software was used to identify the trabecular bone in the tibia. CTvox software was used to visualise the obtained images in a 3D form.

For *in vivo* μCT, the University of Liverpool's centre of preclinical imaging provided the imaging services using the Quantum GX-2 system (PerkinElmer, Inc. Waltham, MA). Whole-body scan images were acquired with the protocol FOV72, high speed, 8 sec x 3. High-resolution scans for upper and lower limbs were performed with the protocol FOV36, high resolution, 4 min.

Locomotor activity monitoring

All mice were housed in a Digital Ventilated Cage (DVC®) rack, equipped with a home cage monitoring system capable of automatically measuring animal activity 24/7 (Iannello, 2019). The DVC® rack is installed on a standard IVC rack (Tecniplast DGM500, Buguggiate, Italy) by adding sensing technologies externally to the cage, so that neither modifications nor intrusion occur in the home cage environment. Animal locomotion activity is monitored via a capacitance sensing technology by means of 12 contactless electrodes, uniformly distributed underneath the cage floor. The 6-week-old WT and cKO mice were monitored for 4 weeks and total distance and average speed of each mouse were measured.

Whole-mount skeletal staining

The whole-mount skeletal staining was done following the Rigueur and Lyons's protocol (Rigueur and Lyons, 2014). Briefly, after dissection, adult mice skeletons were initially kept in 95% ethanol for 4 h before changing the solution and leaving in 95% ethanol overnight at RT. Then, skeletons mice

were kept in acetone for two days at RT. Cartilage staining was performed by immersion in alcian blue for three days; then, mice underwent two changes of 95% ethanol for 4 hours and overnight for destaining. For pre-clearing, skeletons were kept in 1% KOH overnight at 4°C. Bone staining was performed by submersion in alizarin red for five days. Lastly, the final clearing was performed using 1% KOH prior to long-term storage in 100% glycerol.

Double calcein labelling

Double calcein labelling was performed as described previously (van 't Hof et al., 2017). Two intraperitoneal (IP) calcein injections (150 µl/mouse) were given to 5-6 weeks old mice 4 days before culling at an interval of two days. Mice were dissected, and the tibia bones were fixed in natural buffered formalin and kept in 70% ethanol until processing. The bones were dehydrated at 4°C with xylene and decreasing ethanol concentrations. Sample infiltration was performed under vacuum for seven days using a solution containing 88.99% Methyl Methacrylate (MMA), 10% dibutyl phthalate, 1% Perkadox 16 and 0.01% Novoscave. Teflon blocks filled with MMA were used for bone embedding. The blocks were kept at 30 °C in a water bath to polymerise for 18 hours. After that, Historesin was used to attach the embedding rings. Sectioning at 5 µm was performed using the Leica RM2265 microtome. To analyse bone formation, sections were stained without de-plasticisation with 0.1% calcein blue for 3 minutes, dehydrated using different ethanol concentrations and cleared with xylene changes.

Tartrate-resistant acid phosphatase (TRAP) staining

Bone section de-plasticisation was performed by three changes of 2-methoxyethyl acetate (MEA). Section clearing and rehydration were accomplished by xylene and decreasing concentrations of ethanol. TRAP solution was prepared by dissolving naphthol ASTR-phosphate (1.4 mg/ml) and fast red (1.4 mg/ml) in a 0.2 M acetate buffer (pH 5.2) containing 100 mM sodium tartrate. Bone sections were kept in the TRAP solution for 2 hours at 37°C. Then bone sections were counterstained with 0.33 g/l aniline blue and 6 g/l phosphotungstic acid for 15 minutes. The slides were washed with distilled water and then coverslipped with Apathy's serum.

Enzyme-linked immunosorbent assay (ELISA)

Purified human full-length LRP1 (10 nM in 100 µl of 50 mM Tris-HCl (pH 7.5)/150 mM NaCl/10 mM $CaCl_2$, TNC) was coated overnight at 4°C onto microtiter plates (Corning, NY). Wells were blocked with 5% bovine serum albumin in TNC for 24 hours at 4 °C and washed in TNC containing 0.1%

Brij-35 after this and each subsequent step. Wells were then incubated with various concentrations of Wnts in blocking solution for 30 min at RT. Bound proteins were detected using anti-Wnt3a antibody (ab219412, Abcam), anti-Wnt5a antibody (MAB6452, R&D systems) or anti-Wnt11 antibody (ab31962, Abcam) for 1 hour at RT and then with a secondary antibody coupled to horseradish peroxidase for 1 hour at RT. Hydrolysis of tetramethylbenzidine substrate (KPL, Gaithersburg, MA) was measured at 450 nm using a FLUOstar Omega (BMG Labtech). Mean values of technical duplicate were normalized by subtracting the amount of recombinant protein bound to control well that was not coated with LRP1. Extrapolated $K_{D,app}$ values were estimated based on one-phase decay nonlinear fit analysis using GraphPad Prism 9.

Immunocytochemical localisation of Wnt5a and LRP1

WT and LRP1 KO MEFs were generated as described previously (Willnow and Herz, 1994) and kindly provided by Professor Dudley Strickland (University of Maryland School of Medicine). Human normal chondrocytes were prepared as described previously (Yamamoto et al., 2022). Cells were grown with DMEM/F12 containing 10% FBS on 8-well Lab-Tek chamber slides (Nunc Lab-Tek Chamber Slide System, Thermo Scientific) precoated with 0.1% gelatin in PBS overnight. Once reaching confluency, the cells were rested in serum free DMEM/F12 for 24 h. Cells were then incubated in DMEM/F12 containing polymyxin B (50 µg/ml), the broad-spectrum hydroxamate metalloproteinases inhibitor CT1746 (100 µM) and the protease inhibitor cocktail (a mixture of aprotinin, bestatin, E-64, leupeptin and pepstatin A, 1/1000)(SIGMA, P1860) with or without 20 nM Wnt5a in the presence or absence of 500 nM RAP for 3 h at 37 °C. Cells were washed with DMEM/F12 three times and fixed with 4% paraformaldehyde (PFA) in PBS for 10 min at RT. PFA was removed and cells were incubated with 100 mM Glycine for 3 min at RT. Cells were washed with PBS twice and incubated with 0.1% Sudan black in 70% ethanol for 2 minutes. Cells were washed with 70% ethanol twice and PBS once, and permeabilised with in TNC containing 0.1% Triton X-100 for 3 minutes at RT. Cells were incubated with 10% goat serum for 1 hour at RT followed by three times washing with PBS. Each sample was then incubated with anti-Wnt5a antibody (AF645, R&D systems) and anti-LRP1 antibody (ab92544, Abcam) for overnight at 4 °C. Cells were washed with PBS three times and further incubated with Alexa Fluor 488-conjugated anti-mouse IgG and Alexa Fluor 568-conjugated anti-rabbit IgG (Molecular Probes, Eugene, OR) for one hour at RT. Actin was stained with Actin-stain 670 phalloidin (Cell Signalling). Cells were washed with PBS five times and mounted with VECTASHEILD antifade mounting media containing DAPI (2BScientific, Oxford, UK). Immunofluorescence images were acquired using a Zeiss LSM

800 confocal microscope (Zeiss, Oberkochen, Germany). Images were processed using Zen 2.6 (blue edition, Zeiss). For the three-dimensional image visualisation, the delineated region of z-stack image was loaded into the Imaris 10.0.1 software (Bitplane, Belfast, Northern Ireland, UK). The software was used to generate new spots layer. In this layer, LRP1 (red), Wnt5a (green) and DAPI (blue) channels were separately segmented. Slice view was used to measure spot diameter using the line tool and quality above 4.57 and 11.2 were used for LRP1 and Wnt5a, respectively.

Monitoring exogenously added Wnt5a levels in the cell culture

For 0-24 hours incubation assay, WT and LRP1 KO MEFs, and human chondrocytes (5 x 10^3/well) were grown in 24 well plate (pre-coated with 0.1% gelatin for overnight) until cells reach confluent. Cells were then incubated with DMEM/F12 for overnight. The medium was replaced with 0.5 ml of fresh DMEM/F12 containing polymyxin B (50 µg/ml), CT1746 (100 µM) and the protease inhibitor cocktail (1/1000) with or without 20 nM Wnt5a in the presence or absence of 500 nM RAP. After 0-24 hours, 0.5 ml of medium were collected, and the protein was precipitated with trichloroacetic acid and dissolved in 40 µl of 1x SDS-sample buffer (50 mM Tris-HCl pH 6.8, 10 mM dithiothreitol, 2% SDS and 10% glycerol). Cells were washed with PBS once and lysed with 100 µl (for MEFs) or 50 µl (for chondrocytes) of 2x SDS-sample buffer. 12.5 µl of cell lysate and 5 µl (for MEFs) or 10 µl (for chondrocytes) of medium samples were analysed by SDS-PAGE under reducing conditions and underwent Western blotting using anti-Wnt5a antibody (MAB6452, R&D systems). Immune signals for exogenously added Wnt5a in the medium and cell lysate were quantified using ImageJ. Average actin signal was taken as 1 and Wnt5a signal in the cell lysate was normalised against each actin signal. The amount of Wnt5a after 24-h incubation was expressed as a % of the amount of Wnt5a after 3 hours (for MEFs) or 1 hour (for chondrocyte) incubation. For 0-60 minutes incubation assay, WT and LRP1 KO MEFs (5 x 10^3/well) were grown in 96 well plate (pre-coated with 0.1% gelatin for overnight) until cells reach confluent. Cells were then incubated with DMEM/F12 for overnight. The medium was replaced with 50 µl of fresh DMEM/F12 containing polymyxin B (50 µg/ml), CT1746 (100 µM) and the protease inhibitor cocktail (1/1000) with or without 20 nM Wnt5a. After 0-60 minutes h, medium was removed, cells were washed with PBS once and lysed with 30 µl of 2x SDS-sample buffer. 10 µl of cell lysate samples were analysed by SDS-PAGE as described as above. Wnt5a immune signals in the cell lysate were quantified and normalised as described above and the amount of Wnt5a before incubation was taken as 100%.

Statistical analysis

The GraphPad software program was used for statistical analysis. Significance was calculated using the unpaired Student's t-test to compare each group and displayed on the statistical charts as * $p<0.05$, ** $p<0.001$, *** $p<0.001$ and **** $p<0.0001$. A two-way ANOVA was used for the comparison of cell-associated Wnt5a levels between WT and LRP1 KO MEFs after 5-30 min incubation. The data were represented as mean ±SD.

Acknowledgments

We would like to thank Professor Andrew Pitsillides (Royal Veterinary College), Professor Philippa Francis-West (Kings College London), Professor Grant Wheeler (University of East Anglia), Professor Dudley Strickland (University of Maryland School of Medicine), Dr Salvatore Santamaria (University of Surrey), Professor Terence Capellini (Harvard University) and Dr Kathryn Scott for helpful discussions during the writing of this manuscript. The Authors are grateful to the staff at the Biomedical Services, the Histology Units and the Centre for Preclinical Imaging imaging facilities provided by Liverpool Shared Research Facilities, Faculty of Health and Life Sciences, University of Liverpool.

This work was supported by the ministry of education of the Kingdom of Saudi Arabia (to M.A.), Versus Arthritis Career Development Fellowship (21447 to K.Y.), Libyan Ministry of Higher Education and Scientific Research (to A. ME. G) and Qatar National Research Fund (to N. A. AM).

Author Contributions: M Alhashmi performed the experiments, acquired the data and wrote the manuscript. AME Gremida performed the immunobiological and confocal microscopy experiments. NA Maslamani performed the immunobiological experiments and movie editing. K Liu, H Sutherland and P Wilson performed the in vivo experiments and acquired the data. R van't Hof directed the µCT analysis. P Clegg provided financial support for the project and edited the manuscript. G Bou-Gharios and K Yamamoto designed the experiments, wrote and edited the manuscript. K Yamamoto performed the experiments, acquired the data, designed the experiments, wrote and edited the manuscript. All authors reviewed and revised the manuscript.

Competing Interest Statement: The authors declare that there are no conflicts of interests.

All supplementary materials can be found in a single supplementary information file.

References

Akiyama, H., Chaboissier, M.C., Martin, J.F., Schedl, A., and de Crombrugghe, B. (2002). The transcription factor Sox9 has essential roles in successive steps of the chondrocyte differentiation pathway and is required for expression of Sox5 and Sox6. Genes Dev *16*, 2813-2828.

Andre, P., Wang, Q., Wang, N., Gao, B., Schilit, A., Halford, M.M., Stacker, S.A., Zhang, X., and Yang, Y. (2012). The Wnt coreceptor Ryk regulates Wnt/planar cell polarity by modulating the degradation of the core planar cell polarity component Vangl2. J Biol Chem *287*, 44518-44525.

Barnes, H., Larsen, B., Tyers, M., and van Der Geer, P. (2001). Tyrosine-phosphorylated low density lipoprotein receptor-related protein 1 (Lrp1) associates with the adaptor protein SHC in SRC-transformed cells. J Biol Chem *276*, 19119-19125.

Bartelt, A., Behler-Janbeck, F., Beil, F.T., Koehne, T., Muller, B., Schmidt, T., Heine, M., Ochs, L., Yilmaz, T., Dietrich, M.*, et al.* (2018). Lrp1 in osteoblasts controls osteoclast activity and protects against osteoporosis by limiting PDGF-RANKL signaling. Bone Res *6*, 4.

Bi, W., Deng, J.M., Zhang, Z., Behringer, R.R., and de Crombrugghe, B. (1999). Sox9 is required for cartilage formation. Nat Genet *22*, 85-89.

Boucher, P., Gotthardt, M., Li, W.P., Anderson, R.G., and Herz, J. (2003). LRP: role in vascular wall integrity and protection from atherosclerosis. Science *300*, 329-332.

Boucher, P., Liu, P., Gotthardt, M., Hiesberger, T., Anderson, R.G., and Herz, J. (2002). Platelet-derived growth factor mediates tyrosine phosphorylation of the cytoplasmic domain of the low Density lipoprotein receptor-related protein in caveolae. J Biol Chem *277*, 15507-15513.

Bres, E.E., and Faissner, A. (2019). Low Density Receptor-Related Protein 1 Interactions With the Extracellular Matrix: More Than Meets the Eye. Front Cell Dev Biol *7*, 31.

Briggs, M.D., Hoffman, S.M., King, L.M., Olsen, A.S., Mohrenweiser, H., Leroy, J.G., Mortier, G.R., Rimoin, D.L., Lachman, R.S., Gaines, E.S.*, et al.* (1995). Pseudoachondroplasia and multiple epiphyseal dysplasia due to mutations in the cartilage oligomeric matrix protein gene. Nat Genet *10*, 330-336.

Carreca, A.P., Pravata, V.M., Markham, M., Bonelli, S., Murphy, G., Nagase, H., Troeberg, L., and Scilabra, S.D. (2020). TIMP-3 facilitates binding of target metalloproteinases to the endocytic receptor LRP-1 and promotes scavenging of MMP-1. Sci Rep *10*, 12067.

Church, V., Nohno, T., Linker, C., Marcelle, C., and Francis-West, P. (2002). Wnt regulation of chondrocyte differentiation. J Cell Sci *115*, 4809-4818.

Church, V.L., and Francis-West, P. (2002). Wnt signalling during limb development. Int J Dev Biol *46*, 927-936.

Cserjesi, P., Lilly, B., Bryson, L., Wang, Y., Sassoon, D.A., and Olson, E.N. (1992). MHox: a mesodermally restricted homeodomain protein that binds an essential site in the muscle creatine kinase enhancer. Development *115*, 1087-1101.

Ding, Y., Xian, X., Holland, W.L., Tsai, S., and Herz, J. (2016). Low-Density Lipoprotein Receptor-Related Protein-1 Protects Against Hepatic Insulin Resistance and Hepatic Steatosis. EBioMedicine *7*, 135-145.

Galea, G.L., Zein, M.R., Allen, S., and Francis-West, P. (2021). Making and shaping endochondral and intramembranous bones. Dev Dyn *250*, 414-449.

Gao, B., Song, H., Bishop, K., Elliot, G., Garrett, L., English, M.A., Andre, P., Robinson, J., Sood, R., Minami, Y.*, et al.* (2011). Wnt signaling gradients establish planar cell polarity by inducing Vangl2 phosphorylation through Ror2. Dev Cell *20*, 163-176.

Green, J.L., Kuntz, S.G., and Sternberg, P.W. (2008). Ror receptor tyrosine kinases: orphans no more. Trends Cell Biol *18*, 536-544.

Hamlin, A.N., Basford, J.E., Jaeschke, A., and Hui, D.Y. (2016). LRP1 Protein Deficiency Exacerbates Palmitate-induced Steatosis and Toxicity in Hepatocytes. J Biol Chem *291*, 16610-16619.

Hartmann, C. (2006). A Wnt canon orchestrating osteoblastogenesis. Trends Cell Biol *16*, 151-158.

Hartmann, C., and Tabin, C.J. (2000). Dual roles of Wnt signaling during chondrogenesis in the chicken limb. Development *127*, 3141-3159.

Haseeb, A., Kc, R., Angelozzi, M., de Charleroy, C., Rux, D., Tower, R.J., Yao, L., Pellegrino da Silva, R., Pacifici, M., Qin, L.*, et al.* (2021). SOX9 keeps growth plates and articular cartilage healthy by inhibiting chondrocyte dedifferentiation/osteoblastic redifferentiation. Proc Natl Acad Sci U S A *118*.

Hecht, J.T., Nelson, L.D., Crowder, E., Wang, Y., Elder, F.F., Harrison, W.R., Francomano, C.A., Prange, C.K., Lennon, G.G., Deere, M.*, et al.* (1995). Mutations in exon 17B of cartilage oligomeric matrix protein (COMP) cause pseudoachondroplasia. Nat Genet *10*, 325-329.

Henry, S.P., Jang, C.W., Deng, J.M., Zhang, Z., Behringer, R.R., and de Crombrugghe, B. (2009). Generation of aggrecan-CreERT2 knockin mice for inducible Cre activity in adult cartilage. Genesis *47*, 805-814.

Herz, J., Clouthier, D.E., and Hammer, R.E. (1992). LDL receptor-related protein internalizes and degrades uPA-PAI-1 complexes and is essential for embryo implantation. Cell *71*, 411-421.

Hofmann, S.M., Zhou, L., Perez-Tilve, D., Greer, T., Grant, E., Wancata, L., Thomas, A., Pfluger, P.T., Basford, J.E., Gilham, D.*, et al.* (2007). Adipocyte LDL receptor-related protein-1 expression modulates postprandial lipid transport and glucose homeostasis in mice. The Journal of clinical investigation *117*, 3271-3282.

Hu, L., Boesten, L.S., May, P., Herz, J., Bovenschen, N., Huisman, M.V., Berbee, J.F., Havekes, L.M., van Vlijmen, B.J., and Tamsma, J.T. (2006). Macrophage low-density lipoprotein receptor-related protein deficiency enhances atherosclerosis in ApoE/LDLR double knockout mice. Arterioscler Thromb Vasc Biol *26*, 2710-2715.

Iannello, F. (2019). Non-intrusive high throughput automated data collection from the home cage. Heliyon *5*, e01454.

Kawanami, A., Matsushita, T., Chan, Y.Y., and Murakami, S. (2009). Mice expressing GFP and CreER in osteochondro progenitor cells in the periosteum. Biochem Biophys Res Commun *386*, 477-482.

Kawata, K., Kubota, S., Eguchi, T., Aoyama, E., Moritani, N.H., Kondo, S., Nishida, T., and Takigawa, M. (2012). Role of LRP1 in transport of CCN2 protein in chondrocytes. Journal of cell science *125*, 2965-2972.

Laatsch, A., Panteli, M., Sornsakrin, M., Hoffzimmer, B., Grewal, T., and Heeren, J. (2012). Low density lipoprotein receptor-related protein 1 dependent endosomal trapping and recycling of apolipoprotein E. PLoS One *7*, e29385.

Logan, M., Martin, J.F., Nagy, A., Lobe, C., Olson, E.N., and Tabin, C.J. (2002). Expression of Cre Recombinase in the developing mouse limb bud driven by a Prxl enhancer. Genesis *33*, 77-80.

Loukinova, E., Ranganathan, S., Kuznetsov, S., Gorlatova, N., Migliorini, M.M., Loukinov, D., Ulery, P.G., Mikhailenko, I., Lawrence, D.A., and Strickland, D.K. (2002). Platelet-derived growth factor (PDGF)-induced tyrosine phosphorylation of the low density lipoprotein receptor-related protein (LRP). Evidence for integrated co-receptor function betwenn LRP and the PDGF. J Biol Chem *277*, 15499-15506.

Lu, D., Li, J., Liu, H., Foxa, G.E., Weaver, K., Li, J., Williams, B.O., and Yang, T. (2018). LRP1 Suppresses Bone Resorption in Mice by Inhibiting the RANKL-Stimulated NF-kappaB and p38 Pathways During Osteoclastogenesis. J Bone Miner Res *33*, 1773-1784.

Mao, H., Lockyer, P., Townley-Tilson, W.H., Xie, L., and Pi, X. (2016). LRP1 Regulates Retinal Angiogenesis by Inhibiting PARP-1 Activity and Endothelial Cell Proliferation. Arterioscler Thromb Vasc Biol *36*, 350-360.

Mark, P.R., Murray, S.A., Yang, T., Eby, A., Lai, A., Lu, D., Zieba, J., Rajasekaran, S., VanSickle, E.A., Rossetti, L.Z.*, et al.* (2022). Autosomal recessive LRP1-related syndrome featuring cardiopulmonary dysfunction, bone dysmorphology, and corneal clouding. Cold Spring Harb Mol Case Stud *8*.

Martin, J.F., and Olson, E.N. (2000). Identification of a prx1 limb enhancer. Genesis *26*, 225-229.

Mogensen, E.H., Poulsen, E.T., Thogersen, I.B., Yamamoto, K., Bruel, A., and Enghild, J.J. (2022). The low-density lipoprotein receptor-related protein 1 (LRP1) interactome in the human cornea. Exp Eye Res *219*, 109081.

Muratoglu, S.C., Belgrave, S., Hampton, B., Migliorini, M., Coksaygan, T., Chen, L., Mikhailenko, I., and Strickland, D.K. (2013). LRP1 protects the vasculature by regulating levels of connective tissue growth factor and HtrA1. Arterioscler Thromb Vasc Biol *33*, 2137-2146.

Nakajima, C., Haffner, P., Goerke, S.M., Zurhove, K., Adelmann, G., Frotscher, M., Herz, J., Bock, H.H., and May, P. (2014). The lipoprotein receptor LRP1 modulates sphingosine-1-phosphate signaling and is essential for vascular development. Development *141*, 4513-4525.

Ohkawara, B., Glinka, A., and Niehrs, C. (2011). Rspo3 binds syndecan 4 and induces Wnt/PCP signaling via clathrin-mediated endocytosis to promote morphogenesis. Dev Cell *20*, 303-314.

Ono, N., Balani, D.H., and Kronenberg, H.M. (2019). Stem and progenitor cells in skeletal development. Curr Top Dev Biol *133*, 1-24.

Overton, C.D., Yancey, P.G., Major, A.S., Linton, M.F., and Fazio, S. (2007). Deletion of macrophage LDL receptor-related protein increases atherogenesis in the mouse. Circ Res *100*, 670-677.

Pinson, K.I., Brennan, J., Monkley, S., Avery, B.J., and Skarnes, W.C. (2000). An LDL-receptor-related protein mediates Wnt signalling in mice. Nature *407*, 535-538.

Ren, Q., Chen, J., and Liu, Y. (2021). LRP5 and LRP6 in Wnt Signaling: Similarity and Divergence. Front Cell Dev Biol *9*, 670960.

Rigueur, D., and Lyons, K.M. (2014). Whole-mount skeletal staining. Methods Mol Biol *1130*, 113-121.

Roebroek, A.J., Reekmans, S., Lauwers, A., Feyaerts, N., Smeijers, L., and Hartmann, D. (2006). Mutant Lrp1 knock-in mice generated by recombinase-mediated cassette exchange reveal differential importance of the NPXY motifs in the intracellular domain of LRP1 for normal fetal development. Mol Cell Biol *26*, 605-616.

Sato, A., Yamamoto, H., Sakane, H., Koyama, H., and Kikuchi, A. (2010). Wnt5a regulates distinct signalling pathways by binding to Frizzled2. Embo J *29*, 41-54.

Scilabra, S.D., Troeberg, L., Yamamoto, K., Emonard, H., Thogersen, I., Enghild, J.J., Strickland, D.K., and Nagase, H. (2013a). Differential regulation of extracellular tissue inhibitor of metalloproteinases-3 levels by cell membrane-bound and shed low density lipoprotein receptor-related protein 1. J Biol Chem *288*, 332-342.

Scilabra, S.D., Troeberg, L., Yamamoto, K., Emonard, H., Thogersen, I., Enghild, J.J., Strickland, D.K., and Nagase, H. (2013b). Differential regulation of extracellular tissue inhibitor of metalloproteinases-3 levels by cell membrane-bound and shed low density lipoprotein receptor-related protein 1. The Journal of biological chemistry *288*, 332-342.

Scilabra, S.D., Yamamoto, K., Pigoni, M., Sakamoto, K., Muller, S.A., Papadopoulou, A., Lichtenthaler, S.F., Troeberg, L., Nagase, H., and Kadomatsu, K. (2017). Dissecting the interaction between tissue inhibitor of metalloproteinases-3 (TIMP-3) and low density lipoprotein receptor-

related protein-1 (LRP-1): Development of a "TRAP" to increase levels of TIMP-3 in the tissue. Matrix Biol *59*, 69-79.

Shea, C.A., Rolfe, R.A., and Murphy, P. (2015). The importance of foetal movement for co-ordinated cartilage and bone development in utero : clinical consequences and potential for therapy. Bone Joint Res *4*, 105-116.

Sims, A.M., Shephard, N., Carter, K., Doan, T., Dowling, A., Duncan, E.L., Eisman, J., Jones, G., Nicholson, G., Prince, R.*, et al.* (2008). Genetic analyses in a sample of individuals with high or low BMD shows association with multiple Wnt pathway genes. J Bone Miner Res *23*, 499-506.

Strickland, D.K., Gonias, S.L., and Argraves, W.S. (2002). Diverse roles for the LDL receptor family. Trends Endocrinol Metab *13*, 66-74.

Svensson, L., Aszodi, A., Heinegard, D., Hunziker, E.B., Reinholt, F.P., Fassler, R., and Oldberg, A. (2002). Cartilage oligomeric matrix protein-deficient mice have normal skeletal development. Mol Cell Biol *22*, 4366-4371.

Tamai, K., Semenov, M., Kato, Y., Spokony, R., Liu, C., Katsuyama, Y., Hess, F., Saint-Jeannet, J.P., and He, X. (2000). LDL-receptor-related proteins in Wnt signal transduction. Nature *407*, 530-535.

Troeberg, L., Fushimi, K., Khokha, R., Emonard, H., Ghosh, P., and Nagase, H. (2008). Calcium pentosan polysulfate is a multifaceted exosite inhibitor of aggrecanases. Faseb J *22*, 3515-3524.

van 't Hof, R.J., Rose, L., Bassonga, E., and Daroszewska, A. (2017). Open source software for semi-automated histomorphometry of bone resorption and formation parameters. Bone *99*, 69-79.

van Amerongen, R., Fuerer, C., Mizutani, M., and Nusse, R. (2012). Wnt5a can both activate and repress Wnt/beta-catenin signaling during mouse embryonic development. Dev Biol *369*, 101-114.

Vi, L., Baht, G.S., Soderblom, E.J., Whetstone, H., Wei, Q., Furman, B., Puviindran, V., Nadesan, P., Foster, M., Poon, R.*, et al.* (2018). Macrophage cells secrete factors including LRP1 that orchestrate the rejuvenation of bone repair in mice. Nat Commun *9*, 5191.

Wang, Y., Chang, H., Rattner, A., and Nathans, J. (2016). Frizzled Receptors in Development and Disease. Curr Top Dev Biol *117*, 113-139.

Willnow, T.E., and Herz, J. (1994). Genetic deficiency in low density lipoprotein receptor-related protein confers cellular resistance to Pseudomonas exotoxin A. Evidence that this protein is required for uptake and degradation of multiple ligands. Journal of cell science *107 (Pt 3)*, 719-726.

Yamaguchi, T.P., Bradley, A., McMahon, A.P., and Jones, S. (1999). A Wnt5a pathway underlies outgrowth of multiple structures in the vertebrate embryo. Development *126*, 1211-1223.

Yamamoto, K., Okano, H., Miyagawa, W., Visse, R., Shitomi, Y., Santamaria, S., Dudhia, J., Troeberg, L., Strickland, D.K., Hirohata, S.*, et al.* (2016). MMP-13 is constitutively produced in human chondrocytes and co-endocytosed with ADAMTS-5 and TIMP-3 by the endocytic receptor LRP1. Matrix Biol *56*, 57-73.

Yamamoto, K., Owen, K., Parker, A.E., Scilabra, S.D., Dudhia, J., Strickland, D.K., Troeberg, L., and Nagase, H. (2014). Low density lipoprotein receptor-related protein 1 (LRP1)-mediated endocytic clearance of a disintegrin and metalloproteinase with thrombospondin motifs-4 (ADAMTS-4): functional differences of non-catalytic domains of ADAMTS-4 and ADAMTS-5 in LRP1 binding. J Biol Chem *289*, 6462-6474.

Yamamoto, K., Santamaria, S., Botkjaer, K.A., Dudhia, J., Troeberg, L., Itoh, Y., Murphy, G., and Nagase, H. (2017). Inhibition of Shedding of Low-Density Lipoprotein Receptor-Related Protein 1 Reverses Cartilage Matrix Degradation in Osteoarthritis. Arthritis Rheumatol *69*, 1246-1256.

Yamamoto, K., Scavenius, C., Meschis, M.M., Gremida, A.M.E., Mogensen, E.H., Thogersen, I.B., Bonelli, S., Scilabra, S.D., Jensen, A., Santamaria, S.*, et al.* (2022). A top-down approach to uncover the hidden ligandome of low-density lipoprotein receptor-related protein 1 in cartilage. Matrix Biol *112*, 190-218.

Yamamoto, K., Troeberg, L., Scilabra, S.D., Pelosi, M., Murphy, C.L., Strickland, D.K., and Nagase, H. (2013). LRP-1-mediated endocytosis regulates extracellular activity of ADAMTS-5 in articular cartilage. Faseb J *27*, 511-521.

Yan, W., Zheng, L., Xu, X., Hao, Z., Zhang, Y., Lu, J., Sun, Z., Dai, J., Shi, D., Guo, B.*, et al.* (2022). Heterozygous LRP1 deficiency causes developmental dysplasia of the hip by impairing triradiate chondrocytes differentiation due to inhibition of autophagy. Proc Natl Acad Sci U S A *119*, e2203557119.

Figures

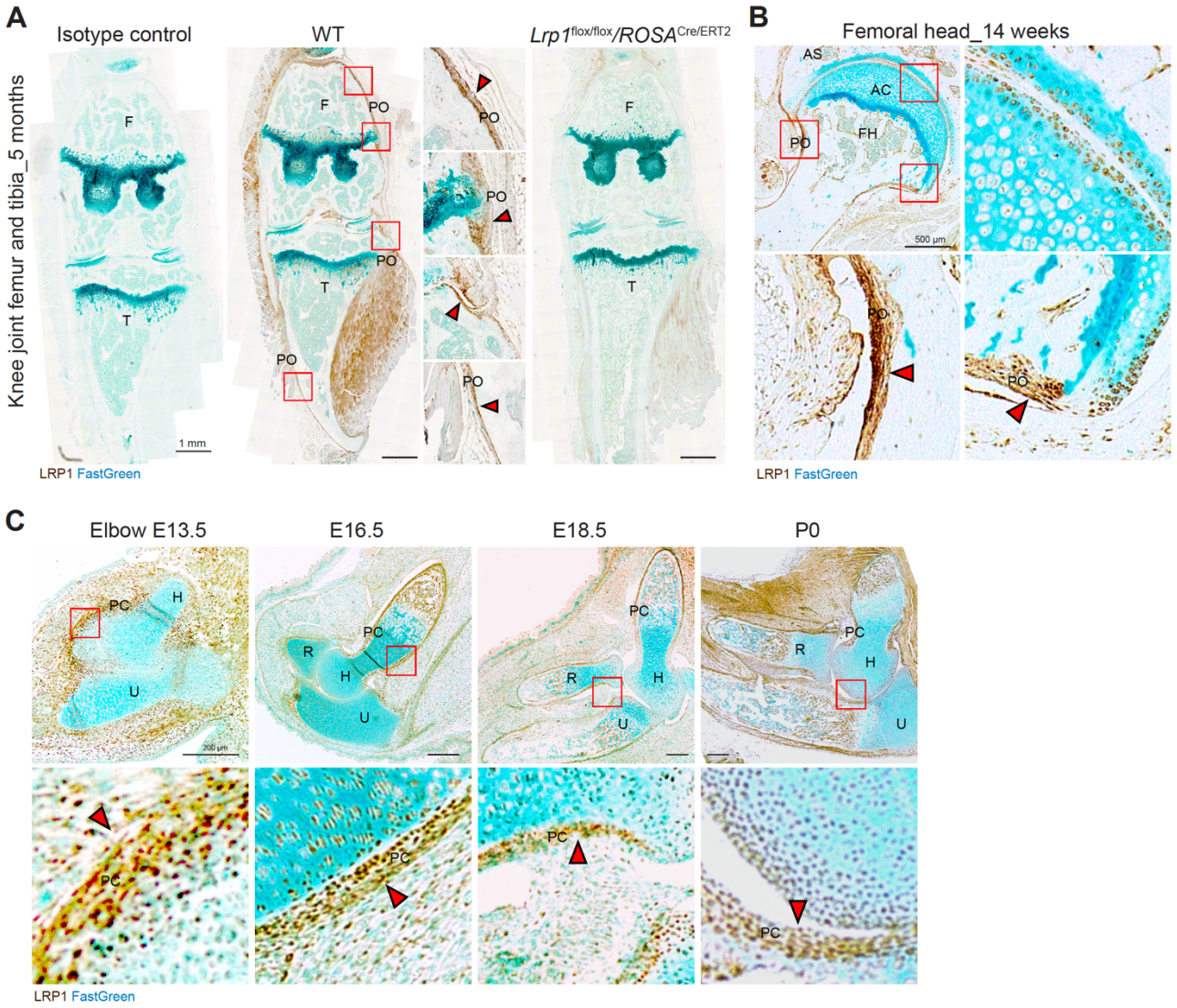

Fig 1. LRP1 is abundantly expressed in periosteal and perichondrial stem cells.
A, Representative automated images of immunohistochemical staining of LRP1 and fast green counterstaining in knee joint sections of 5-month-old *Lrp1*$^{flox/flox}$ (WT) and the inducible pan-tissue *Lrp1* KO mice (*Lrp1*$^{flox/flox}$*/ROSA26*$^{Cre/ERT2}$)(n = 3 each). Scale bar, 1 mm. F, femur; T, tibia; PO, periosteum. *B and C*, Representative images of immunohistochemical staining of LRP1 and fast green counterstaining in 14-week-old hip joint sections (*B*) and E13.5-P0 elbow joint sections (*C*) of WT mice (n = 3 each). Scale bars, 500 µm (*B*) or 200 µm (*C*). IF, inter frontal; C, coronal; S, sagittal sutures. AS, acetabulum socket; AC, articular cartilage; FH, femur head; H, humerus; R, radius; U, ulna; PC, perichondrium. Regions delineated by the red squares in the panels have been magnified in the right (*A*), surrounded (*B*) and lower (*C*) panels. Arrow heads indicate periosteum (*A* and *B*) and perichondrium (*C*) layers.

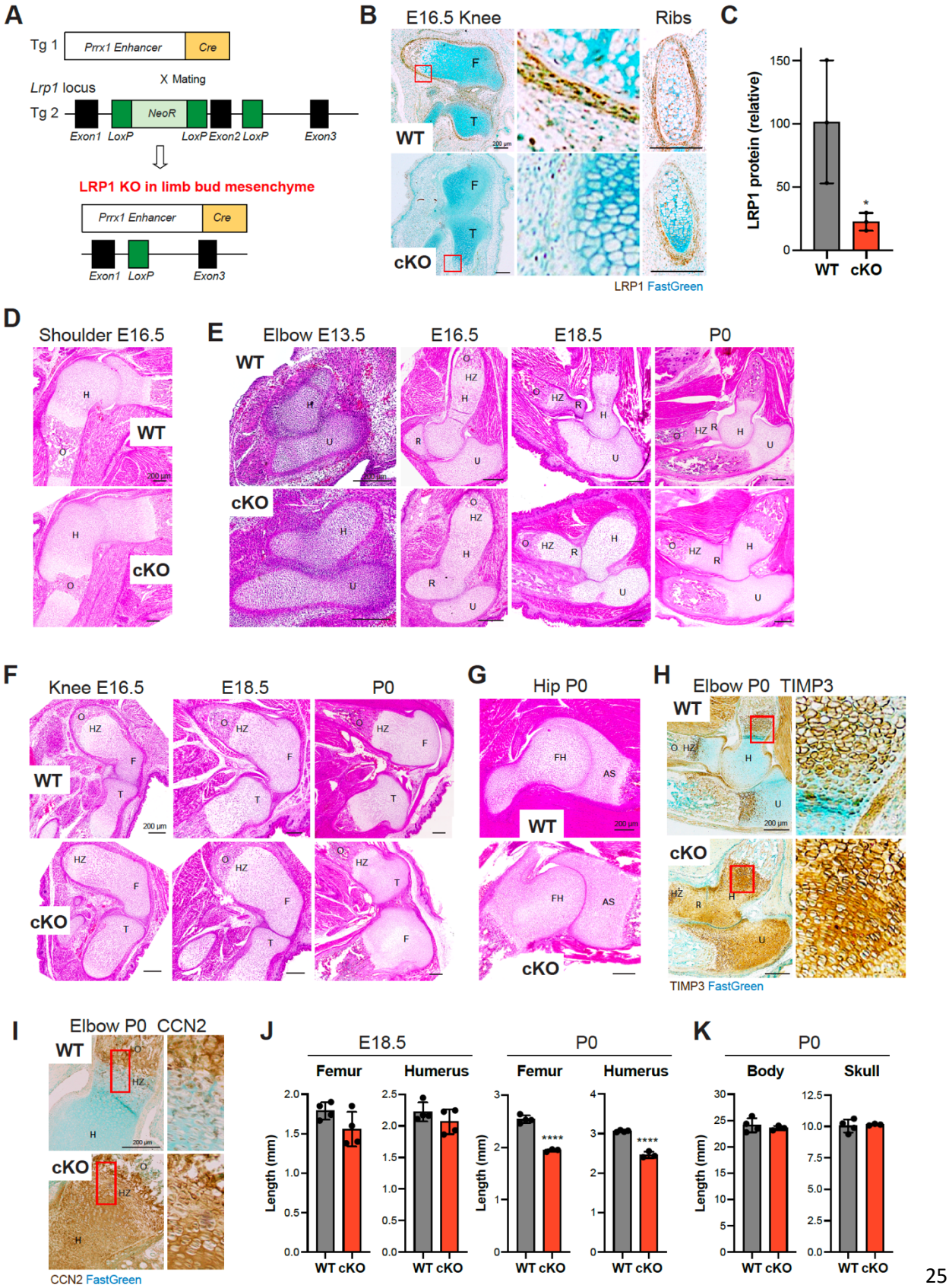
A
Tg 1
Prrx1 Enhancer
Cre
X Mating
Lrp1 locus
Tg 2
NeoR
Exon1 LoxP
LoxP Exon2 LoxP
Exon3
LRP1 KO in limb bud mesenchyme
Prrx1 Enhancer
Cre
Exon1 LoxP
Exon3
B
E16.5 Knee
Ribs
WT
cKO
LRP1 FastGreen
C
LRP1 protein (relative)
WT cKO
D
Shoulder E16.5
WT
cKO
E
Elbow E13.5
E16.5
E18.5
P0
WT
cKO
F
Knee E16.5
E18.5
P0
WT
cKO
G
Hip P0
WT
cKO
H
Elbow P0 TIMP3
WT
cKO
TIMP3 FastGreen
I
Elbow P0 CCN2
WT
cKO
CCN2 FastGreen
J
E18.5
P0
Femur
Humerus
Femur
Humerus
Length (mm)
WT cKO
K
P0
Body
Skull
Length (mm)
WT cKO

Fig 2. Conditional deletion of *Lrp1* in skeletal progenitors impairs early bone and joint formation. *A*, Schematic diagram showing the constructs used to generate limb bud mesenchyme-selective LRP1 conditional knockout mice. Transgenic mouse lines harbouring Prrx1 limb enhancer Cre (Tg 1) and floxed *LRP1* (Tg 2) were used to establish the LRP1Prrx1Cre line. *B*, Representative images of immunohistochemical staining of LRP1 and fast green counterstaining in E16.5 knee and rib sections of WT and *Lrp1*$^{flox/flox}$*/Prrx1*^{Cre} homozygote conditional KO (cKO) mice (n = 3 each). Regions delineated by the red squares in the upper panels have been magnified in the lower panels. Scale bar, 200 μm. F, femur; T, tibia. *C,* Western blot analysis of the cells isolated from long bones of 5-week-old WT and *Lrp1*$^{flox/flox}$*/Prrx1*^{Cre} (cKO) mice using anti-LRP1 antibody. Band intensity was quantified by densitometry and the amount of LRP1 was expressed as a percentage of the amount of WT limb bones, which was taken as 100%. Circles represent individual mice and bars show the mean ± *SD*. *, $p < 0.05$ by 2-tailed Student's t test. *D-G*, Representative images of H&E staining of E16.5 shoulder (*D*), E13.5-P0 elbow (*E*), E16.5-P0 knee (*F*) and P0 hip (*G*) sections of WT and *Lrp1*$^{flox/flox}$*/Prrx1*^{Cre} (cKO) mice (n = 3 each). Scale bar, 200 μm. H, humerus; R, radius; U, ulna; HZ, hypertrophic zone; O, primary ossification center; F, femur; FH, femur head; T, tibia; AS, acetabulum socket. *H* and *I*, Representative images of immunohistochemical staining of TIMP3 and CCN2 and fast green counterstaining in E16.5 knee and rib sections of WT and *Lrp1*$^{flox/flox}$*/Prrx1*^{Cre} homozygote conditional KO (cKO) mice (n = 3 each). Regions delineated by the red squares in the panels have been magnified in the right panels. Scale bar, 200 μm. *J* and *K*, Femur and humerus bone (*J*), body and skull (*K*) length of P0 (*J* and *K*) and E18.5 (*J*) WT and *Lrp1*$^{flox/flox}$*/Prrx1*^{Cre} (cKO) mice. Circles represent individual mice and bars show the mean ± *SD*. *p* values were evaluated by 2-tailed Student's t test. ****, $p < 0.0001$.

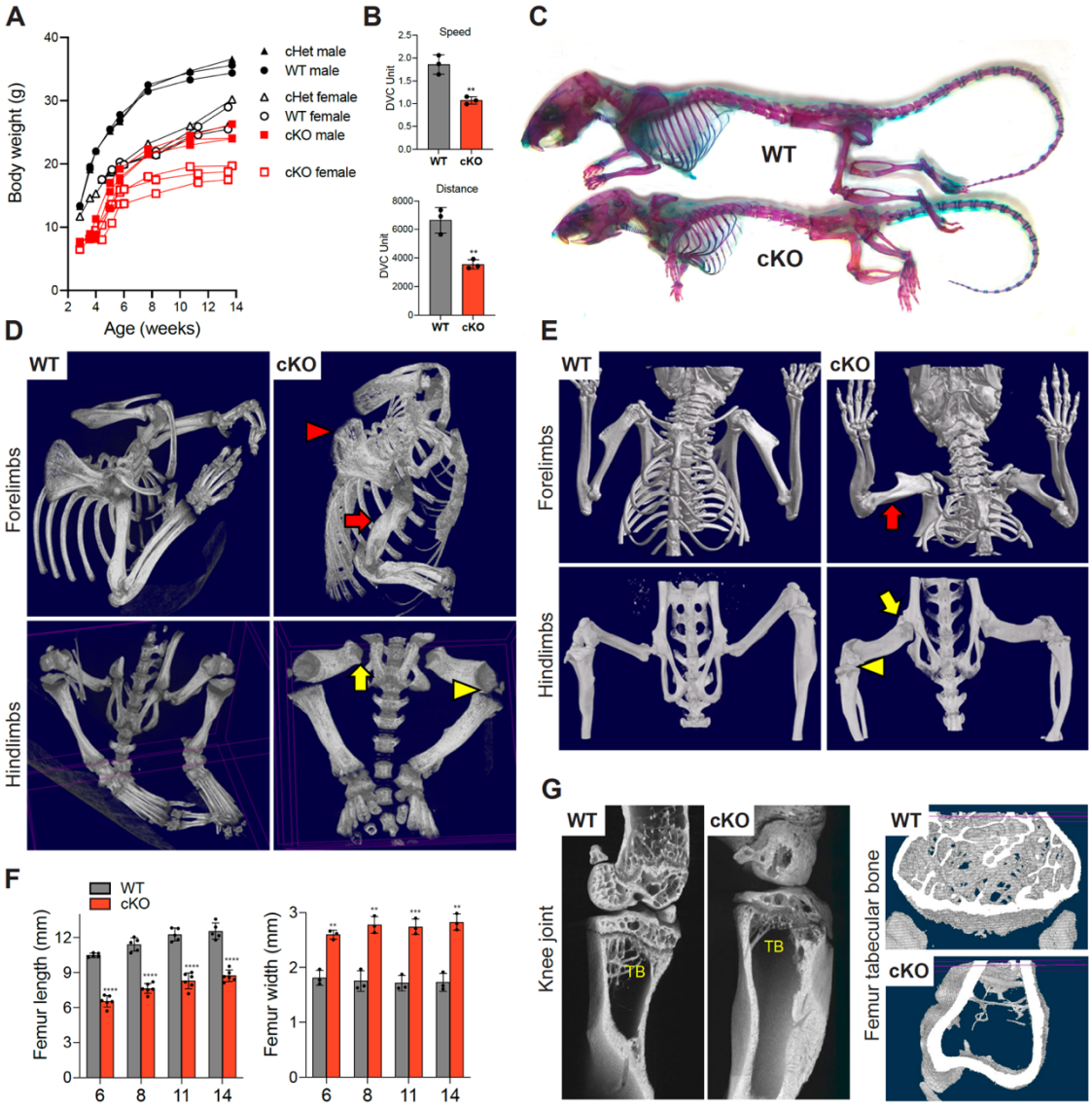

Fig 3. LRP1 deficiency in skeletal progenitors results in dwarfism, impaired mobility and multiple severe skeletal defects.
A, Mouse weight measurement from 3-14 weeks after birth. Closed (male) and open (female) black circles (WT), black triangles (cHet; heterozygote conditional KO), and red squares (cKO) represent individual mice. *B*, Total distance and average speed of WT and *Lrp1*$^{flox/flox}$/*Prrx1*^{Cre} (cKO) mice. Locomotor activity of 6-week-old mice (n = 3 each) measured by the continuous automated home-cage monitoring system for 4 weeks. Circles represent individual mice and bars show the mean ± *SD*. **, $p < 0.01$ by 2-tailed Student's t test. *C*, Whole-mount skeletal staining of 14-week-old mice with Alcian blue and Alizarin red. *D and E*, Representative images of in vivo X-ray analysis of limbs of 2-week-old (*D*) and 14-week-old (*E*) mice (n = 5 each). Red arrowheads and arrows, and yellow arrowheads and arrows indicate shoulder blades, long bones, knee and hip joints in *Lrp1*$^{flox/flox}$/*Prrx1*^{Cre} (cKO) mice, respectively. *F*, Femur bone length and width of 6-14-week-old mice. Circles represent individual mice and bars show the mean ± *SD*. **, $p < 0.01$; ***, $p < 0.001$; ****, $p < 0.0001$ by 2-tailed Student's t test. *G*, Representative images of high-resolution μCT analysis of femur trabecular bones of 14-week-old mice (n = 5 each). TB, trabecular bone.

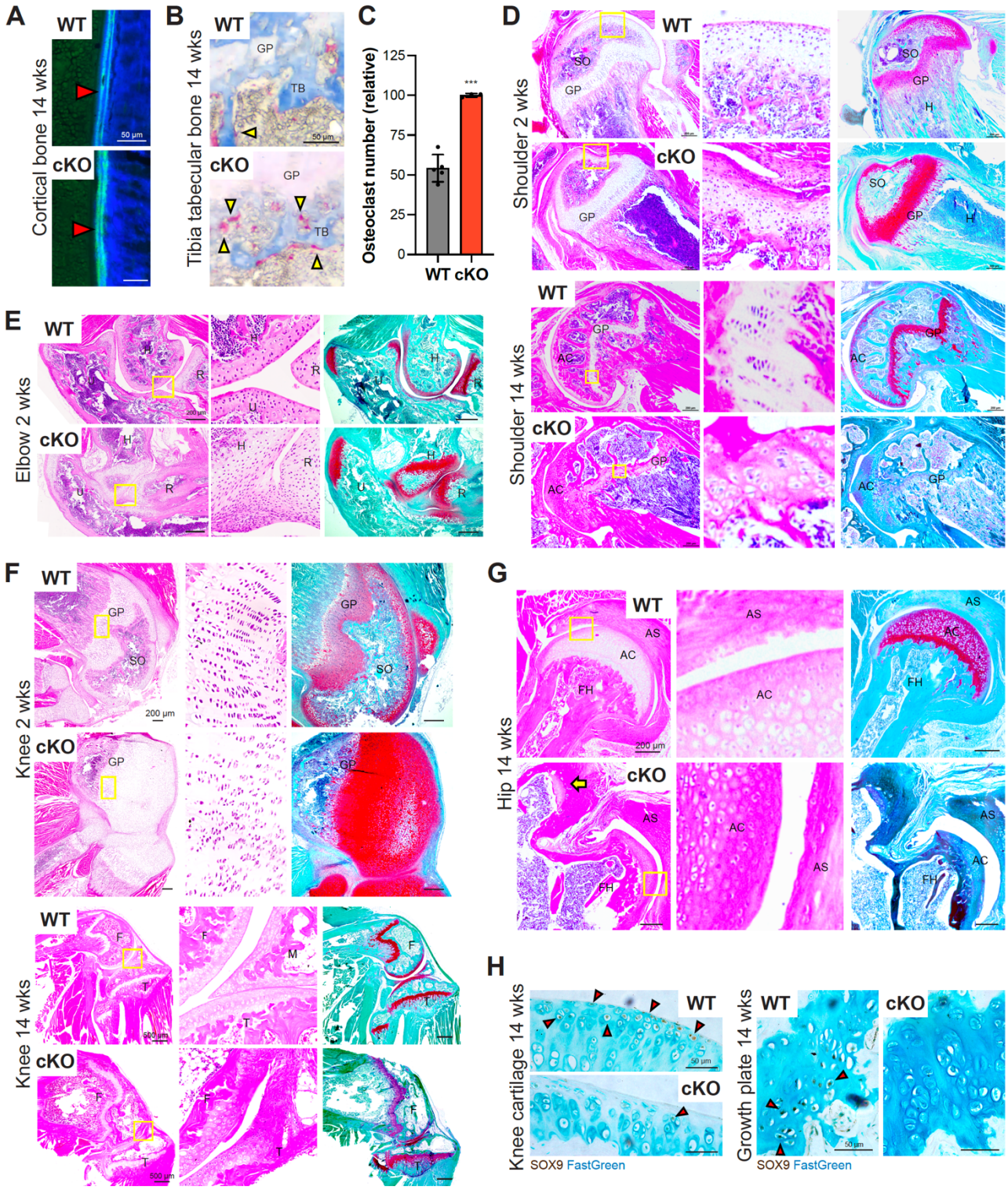
A
WT
cKO
Cortical bone 14 wks
50 µm
B
WT
cKO
Tibia tabecular bone 14 wks
GP
TB
50 µm
C
Osteoclast number (relative)
125
100
75
50
25
0
***
WT cKO
D
WT
cKO
Shoulder 2 wks
SO
GP
H
Shoulder 14 wks
AC
E
WT
cKO
Elbow 2 wks
H
R
U
F
WT
cKO
Knee 2 wks
GP
SO
200 µm
Knee 14 wks
F
T
M
500 µm
G
WT
cKO
Hip 14 wks
AS
AC
FH
200 µm
H
Knee cartilage 14 wks
Growth plate 14 wks
WT
cKO
50 µm
SOX9 FastGreen

Fig 4. LRP1 deficiency in skeletal progenitors disrupts growth plate and columnar chondrocyte organisation, impairs articulation and cavitation, and dysregulates proteoglycan turnover.
A, Representative images of fluorescent microscopy analysis of calcein-double stained cortical bones in 14-week-old mice (n = 3 each). Red arrowheads indicate calcein double staining in cortical bone. Scale bar, 50 µm. *B*, TRAP and aniline blue staining of tibia trabecular bone of 14-week-old mice (n = 3 each). Yellow arrowheads highlight osteoclast staining. Scale bar, 50 µm. TB, trabecular bone; GP, growth plate. *C*, Measurement of osteoclast numbers in WT and *Lrp1*$^{flox/flox}$*/Prrx1*^{Cre} (cKO) trabecular bones. Circles represent individual mice and bars show the mean ± *SD*. ***, $p < 0.001$ by 2-tailed Student's t test. *D*-*G*, Representative images of H&E and safranin-O/fast green staining in shoulder (*D*), elbow (*E*), knee (*F*) and hip (*G*) joint sections of 2- and/or 14-week-old WT and *Lrp1*$^{flox/flox}$*/Prrx1*^{Cre} **(**cKO) mice (n = 3 each). Arrow indicates the extra groove of femoral heads. Scale bar, 200 µm. GP, growth plate; AC, articular cartilage; F, femur; T, tibia; M, menisci. *H*, Representative images of immunohistochemical staining of SOX9 in knee articular cartilage and growth plate sections of 14-week-old WT and *Lrp1*$^{flox/flox}$*/Prrx1*^{Cre} (cKO) mice. Arrow heads indicate cells with SOX9 positive staining. Scale bar, 50 µm.

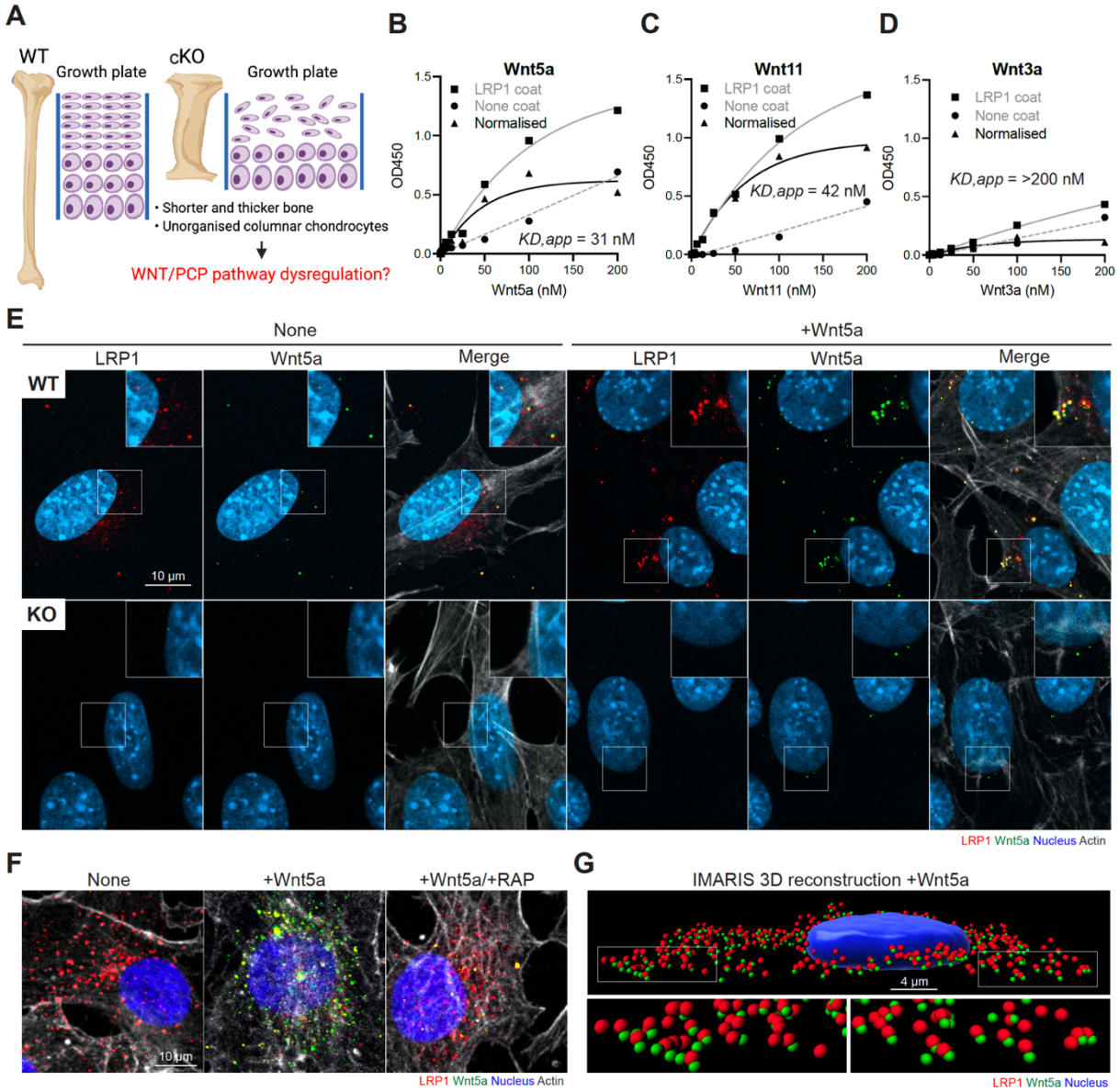

Fig 5. LRP1 directly binds to Wnt5a and Wnt11, key non-canonical WNT pathway components, and mediates endocytosis of Wnt5a.
A, Schematic diagram illustrating the long bone phenotype of *Lrp1*$^{flox/flox}$/*Prrx1*^{Cre} mice. *B-D*, Full-length sLRP1 was coated onto microtiter plates and the binding of 0-200 nM Wnt5a (*B*), Wnt11 (*C*), Wnt3a (*D*) was measured using specific antibody for each Wnt as described under "Materials and Methods". Mean values of technical duplicates for none-coating, LRP1-coating and after normalisation were shown as circles, squares and triangles, respectively. Extrapolated $K_{D,app}$ values were estimated based on one-phase decay nonlinear fit analysis (black lines). *E and F*, Representative images of confocal microscopy analysis for Wnt5a and LRP1 in WT and LRP1 KO MEFs (n = 3) (*E*) or human normal chondrocytes (n = 3) (*F*). Cells were incubated with 20 nM Wnt5a for 3 h in the absence (*G and H*) or presence of 500 nM RAP (*H*). Wnt5a, LRP1, cytoskeleton and nucleus were visualised as described under "Materials and Methods". Scale bar, 10 µm. *I*, Imaris image visualisation of staining of LRP1 and Wnt5a in human chondrocyte incubated with 20 nM Wnt5a for 3 h. Scale bar, 4 µm. Regions delineated by the white squares in the panels have been magnified in the top right bottom (*E*) or the bottom (*G*).

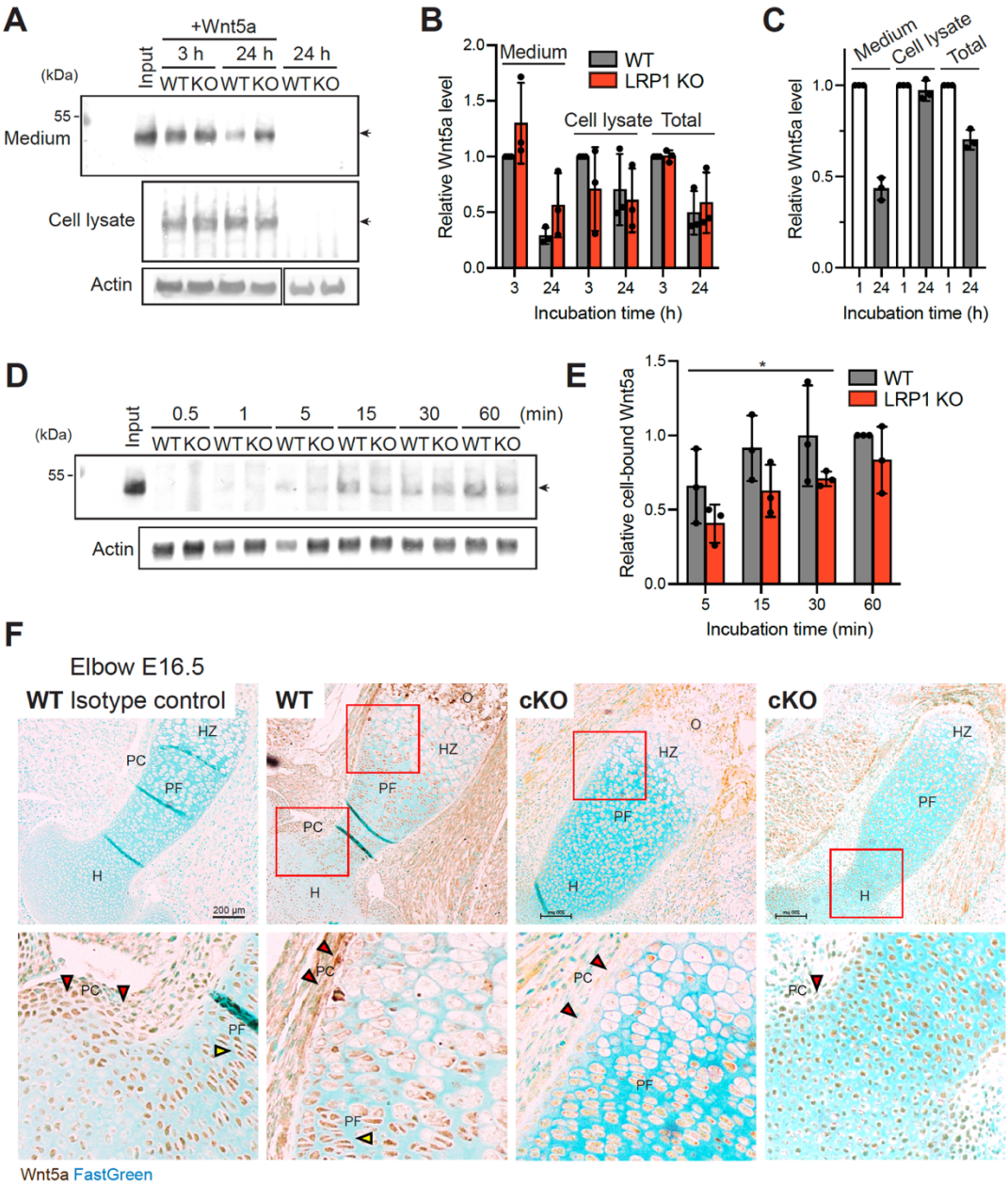

Fig 6. LRP1 facilitates cell-association, endocytic recycling and graded distribution of Wnt5a in the developing limbs.
A and B, WT and LRP1 KO MEFs (n = 3) were incubated with 20 nM Wnt5a for 3-24 h and Wnt5a in the medium and cell lysate were detected by Western blotting (*A*). Densitometric analysis of immunoreactive Wnt5a bands was carried out. The relative amount of Wnt5a in the media, cell lysate and both media and cell lysate (total) were expressed by taking the amount of Wn5a after 3-h incubation in WT MEFs as 1 (*B*). *C*, human normal chondrocytes (n = 3) were incubated with 20 nM Wnt5a for 1-24 h and analysed as in *A* and *B*. The relative amount of Wnt5a after 24-h incubation was expressed by taking the amount of Wn5a after 1-h incubation as 1. Circles represent individual experiment and bars show the mean ± *SD*. *D and E*, WT and LRP1 KO MEFs (n = 3) were incubated with 40 nM Wnt5a for 0.5-60 min and Wnt5a in the cell lysate was detected by Western blotting (*D*). The relative amount of Wnt5a was expressed by taking the amount of

Wnt5a after 60-min incubation as 1 (*E*). Circles represent individual mice and bars show the mean ± *SD*. *p* values for the amount of Wnt5a after incubation for 5-30 min in WT *versus* LRP1 KO MEFs were evaluated by two-way ANOVA. *, $p < 0.05$.). *F*, Representative images of immunohistochemical staining of Wnt5a and fast green counterstaining in E16.5 elbow sections of WT and *Lrp1*$^{flox/flox}$*/Prrx1*^{Cre} (cKO) mice. Scale bar, 200 μm. Regions delineated by the squares in the upper panels have been magnified in the lower panels. Red arrowheads indicate Wnt5a protein in perichondrium. H, humerus; HZ, hypertrophic zone; O, primary ossification center; PF, proliferative flattened chondrocytes; PC, perichondrium.

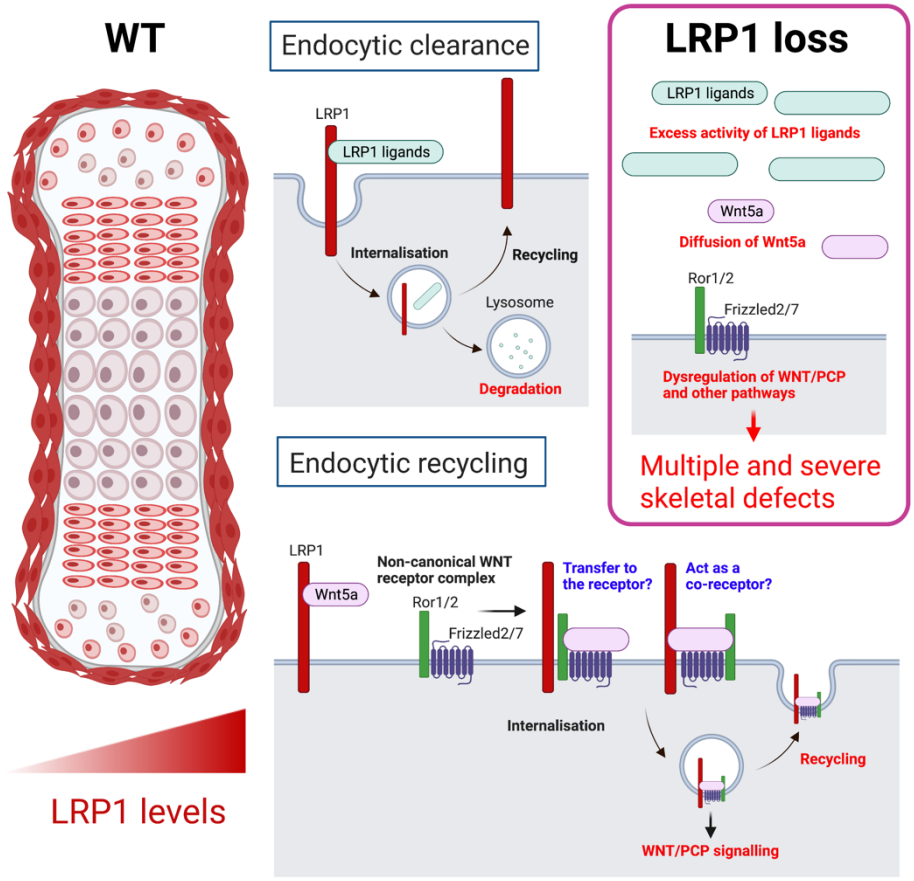

Fig 7. LRP1-mediated endocytic clearance and recycling in endochondral ossification.
Skeletal progenitor LRP1 is likely to have at least two different functions: to remove molecules from extracellular milieu and degrad them intracellularly (endocytic clearance), and to capture, recycle and distribute molecules (endocytic recycling). LRP1 may mediate internalisation of Wnt5a and its receptor complexes to activate WNT/PCP singalling pathway. Thus, loss of LRP1 leads to excess activity of some of LRP1 ligands and erratic concentrations of Wnt5a, resulting in multiple and severe bone and joint defects.